IEICE TRANS. ELECTRON., VOL.E107–C, NO.10 OCTOBER 2024

PAPER *Special Section on Microwave and Millimeter-Wave Technologies*

Experimental Study on Sub-Terahertz Wideband Single-Carrier Transmitter with Pre-Equalizing Frequency Response

Atsushi FUKUDA[†a)], ***Senior Member***, **Hiroto YAMAMOTO**[††], **Junya MATSUDAIRA**[†], **Sumire AOKI**[†], ***Nonmembers***, ***and*** **Yasunori SUZUKI**[†], ***Senior Member***

SUMMARY This paper proposes a novel configuration for a wideband single-carrier transmitter using a sub-terahertz frequency. For wideband single-carrier transmission over a bandwidth of several gigahertz, the frequency response non-flatness derived from transmitter components in an operating band seriously deteriorates the transmission quality due to inter-symbol interference. A promising approach to address this problem is equalizing the frequency response non-flatness at the transmitter. The proposed novel configuration has a feedback route for calculating the inverse frequency response and multiplying it with a transmission signal spectrum in the frequency domain. Moreover, we verify that employing the proposed transmitter configuration simplifies the receiver configuration by lowering the calculation complexity to minimize the inter-symbol interference to meet the signal-to-interference-and-noise ratio requirements. To confirm the feasibility of the proposed configuration, the transmission quality obtained using the proposed configuration is measured and evaluated. Experimental results confirm that the proposed configuration improves the error vector magnitude value to over 5 dB for a 10 Gbaud transmission and the transmission data rate of 25 Gbps.

key words: *sub-THz, single-carrier transmission, wideband transmission, pre-equalization*

1. Introduction

Recently, research and development has been conducted around the world on the 6th generation mobile communications system (6G) [1]–[11]. One 6G requirement is extremely high data rate communications over 100 Gbps [12]. Increasing the number of multi-input and multi-output branches, N, is one approach to achieve high data rate communications [13]. Although the data rate increases in proportion to N, so far it seems that an extremely large N is required to meet the 6G data rate requirement for bandwidths used by the mobile communications systems. On the other hand, according to Shannon's channel capacity equation, since the data rate can be increased in proportion to the bandwidth (BW) of a transmission signal [14], [15], a BW over several gigahertz is considered to meet the 6G capacity requirement [12]. Therefore, sub-terahertz (sub-THz) bands with the center frequency of below 300 GHz are candidates for 6G to assign such a huge BW [16], [17].

There are several challenges in utilizing the sub-THz bands. Since the transmission signals to meet the high data rate requirement for 6G are assumed to have high index modulation schemes, the required signal-to-noise ratio (SNR) becomes high for a high-quality transmission. However, currently available sub-THz power amplifiers (PAs) have a lower output power level and power efficiency than those for lower frequency bands [18]–[22]. It is considered that the required PA output backoff for single-carrier transmission is lower than that for multi-carrier transmission [23]. Therefore, single-carrier transmission is considered to be a candidate transmission scheme for the sub-THz bands because the PA can operate with higher output power level and power efficiency.

A basic transmitter (Tx) is configured with a baseband (BB) part, an intermediate frequency part, and a radio frequency (RF) part. Then, each part comprises cascade connected devices with its own frequency response due to dedicated circuit design schemes and parasitic elements depending on the design frequencies. The frequency response flatness of each Tx component can be designed and achieved individually in conventional narrowband operation. However, it is more difficult to achieve flatness of the total frequency response of the Tx by flattening each of the Tx components in a huge BW over several gigahertz. That is why circuit design schemes with frequency response flatness in the sub-THz bands have not yet been well-established.

The frequency response non-flatness in the BW causes inter-symbol interference (ISI) resulting in serious degradation in the single-carrier transmission quality [24]. Generally, to avoid ISI degradation, employing an equalizer in the receiver (Rx) is a common approach. The equalizer minimizes the ISI caused by frequency selective fading generated in the propagation channel. However, equalizing the ISI caused by not only heavier frequency selective fading in a wider band but also the frequency response non-flatness in the Tx leads to an increase in the required calculation load in the Rx. Then, the increase in the calculation load for the signal with a huge BW results in high power consumption in the Rx. Especially for battery driven mobile terminals, a low power consumption equalizer is necessary for high data rate transmission in the downlink. In order to address these issues, a pre-equalization technique that equalizes the ISI caused by the Tx frequency response non-flatness in the huge BW transmission system must be developed. To the best of our knowledge, a wideband single-carrier Tx with a configuration that achieves frequency response flatness has

Manuscript received October 27, 2023.
Manuscript revised February 9, 2024.
Manuscript publicized April 9, 2024.

[†]NTT DOCOMO, INC., DOCOMO R&D Center, Yokosuka-shi, 239–8536 Japan.
[††]NTT Access Network Service Systems Laboratories, Yokosuka-shi, 239–0847 Japan.
a) E-mail: fukudaats@nttdocomo.com

DOI: 10.1587/transele.2024MMP0007

not yet been proposed [25]–[31].

We propose a wideband single-carrier Tx configuration that implements a functionality for minimizing the ISI caused by the non-flat frequency response resulting from the transmission devices. Based on eye-diagram experimental results, the proposed configuration with a feedback route that multiplies the inverse frequency response to the transmission signal in the frequency domain minimizes the ISI [32]. In this paper, a novel wideband single-carrier transmission system that comprises the proposed Tx with pre-equalization and the conventional Rx with equalization for the propagation channel is proposed. The proposed configuration can compensate for the total frequency response non-flatness of the Tx based on the frequency characteristics of sub-THz components with desired wideband design difficulties using digital assisted techniques. This is the first experimental study to verify that a pre-equalization technique is applicable to minimize the ISI caused by the non-flat frequency response of the systems for wideband single-carrier transmission.

In Sect. 2, details regarding the proposed Tx configuration are given and the principles on pre-equalization are described. In addition, the transmission quality degradation caused by amplitude deviation is evaluated through experiments using wideband single-carrier transmissions. In Sect. 3, the effects of pre-equalization on the wideband transmission quality are verified experimentally using actual sub-THz transmission systems transmitting signals with the maximum BW of 14 GHz. According to the evaluation results regarding the improvement in the signal quality, they show that the novel Tx configuration with pre-equalization is applicable to communication systems transmitting ultra-wideband single-carrier transmission while requiring low complexity.

2. Proposed Tx Configuration

A sub-THz transmission system is required to operate in a huge BW over several gigahertz in order to achieve the high data rates expected for the 6G era. Txs and Rxs, however, have their own frequency responses in the operation band due to implemented devices such as filters, amplifiers, frequency converters, and so on. The proposed pre-equalization Tx is equipped with a function that compensates for the spectrum non-flatness of the single-carrier transmission signal with a huge BW caused by the total frequency response of the Tx. Signal flows to produce the original transmission signal in the Tx are shown in Figs. 1.

Figure 1 (a) shows the signal flow of a conventional Tx without pre-equalization. The transfer function of the Tx, $H_{\mathrm{tx}}(f)$, is applied to an original transmission signal spectrum, $X(f)$, in the frequency domain. Then, the output signal from the Tx becomes $H_{\mathrm{tx}}(f)X(f)$. For a conventional narrowband transmission, since $H_{\mathrm{tx}}(f)$ is considered constant in the operation band, no pre-equalization is required.

For single-carrier transmission schemes, the frequency response non-flatness generates ISI and leads to more serious

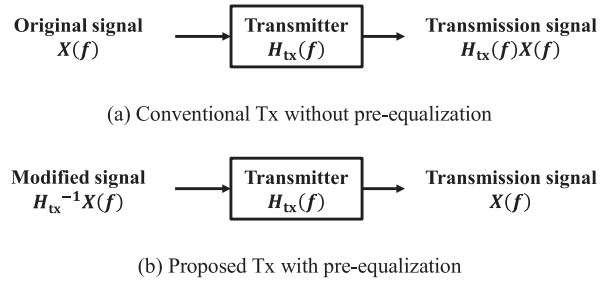

(a) Conventional Tx without pre-equalization

(b) Proposed Tx with pre-equalization

Fig. 1 Signal flows to produce transmission signals, (a) Conventional Tx without pre-equalization and (b) Proposed Tx with pre-equalization.

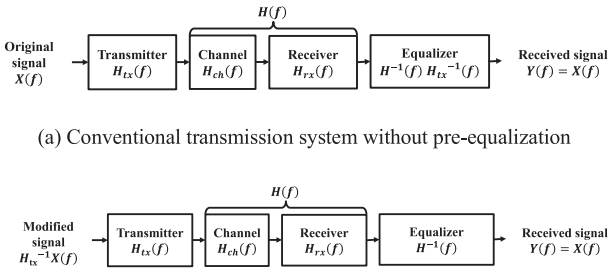

(a) Conventional transmission system without pre-equalization

(b) Proposed transmission system configuration with pre-equalization

Fig. 2 Signal flows to transmit signal with equalizer in Rx, (a) Conventional Tx without pre-equalization and (b) Proposed configuration with pre-equalization.

degradation in the signal quality for a digitally modulated signal. Specially for signal transmission with a huge BW, $H_{\mathrm{tx}}(f)$ is considered to fluctuate in the operation band which deteriorates the signal quality. Therefore, pre-equalization is applied to the original signal. Figure 1 (b) shows the proposed Tx with pre-equalization. The pre-equalization scheme generates a modified signal, $H_{\mathrm{tx}}{}^{-1}(f)X(f)$. Here, $H_{\mathrm{tx}}{}^{-1}(f)$ is the inverse transfer function of $H_{\mathrm{tx}}(f)$. Since the modified signal incurs the effect of $H_{\mathrm{tx}}(f)$ in the Tx, the transmission signal output from the Tx becomes $X(f)$, which is the original transmission signal.

Signal flows to transmit the original transmission signal between the Tx and the Rx are shown in Figs. 2. Generally, an equalizer in the Rx has been used to compensate for the ISI generated by the frequency response in the propagation channel such as frequency selective fading. Moreover, it is possible to equalize the frequency characteristics of the implemented devices in the Rx. Figure 2 (a) shows the signal flow of a conventional transmission system without pre-equalization. Here, the total transfer function of the propagation channel, $H_{\mathrm{ch}}(f)$, and the Rx, $H_{\mathrm{rx}}(f)$ is indicated as $H(f)$. The $H_{\mathrm{tx}}(f)$ and $H(f)$ are applied to $X(f)$ in the frequency domain. Therefore, the equalizer in the Rx applies the inverse function of $H_{\mathrm{tx}}(f)$ and $H(f)$, $H^{-1}(f)H_{\mathrm{rx}}{}^{-1}(f)$, to the input signal and produces $X(f)$ as the received signal, $Y(f)$. Figure 2 (b) shows the proposed transmission system with pre-equalization. Since the pre-equalization scheme generates $H_{\mathrm{tx}}{}^{-1}(f)X(f)$, the equalizer in the Rx applies only the $H^{-1}(f)$ to the input signal and produces $X(f)$ as the

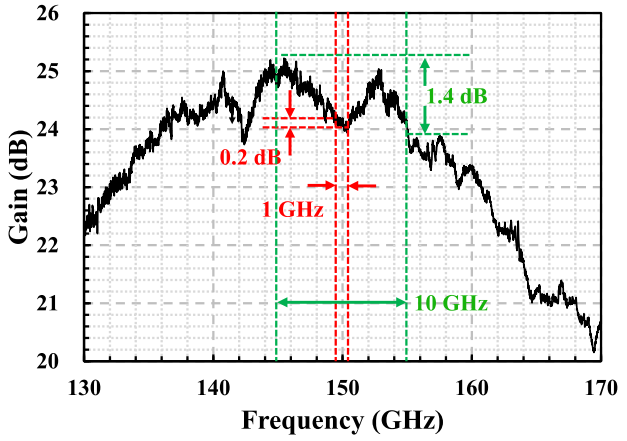

Fig. 3 Measured characteristics for small signal gain of commercially available D-band amplifier.

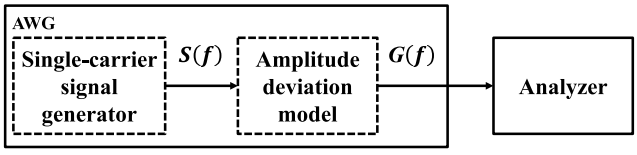

Fig. 4 Experimental investigation system.

received signal. Therefore, the equalizer can be designed regardless of the frequency response non-flatness of the Tx.

Figure 3 shows measured frequency characteristics for a small signal gain of a commercially available D-band amplifier as one example that causes the frequency response non-flatness. According to Fig. 3, the gain decreases gradually as the frequency increases. For example, when the transmission signal has a BW of 1 GHz at the center frequency of 150 GHz, the gain deviation is 0.2 dB. However, the gain deviation is 1.4 dB for the BW of 10 GHz and becomes larger than that for 1 GHz. The difference in the amplifier gain results in frequency response non-flatness in the operation band.

Generally, when the transmitted signal spectrum is $S(f)$, received signal spectrum, $G(f)$, with amplitude deviation is expressed by the following equation.

$$G(f) = S(f)10^{\frac{\{a_1(fT)+a_2(fT)^2+\cdots\}}{20}} \tag{1}$$

where a_n is the n-th order amplitude deviation in the operation BW expressed in decibels and T is the clock period. The degradation in the signal quality due to the first-order amplitude deviation is investigated experimentally. Figure 4 shows the employed experimental system configuration for the amplitude deviations. An arbitrary waveform generator (AWG) generates a single-carrier signal and then amplitude deviations are applied to the signal. After amplitude deviation occurs, error vector magnitude with root mean square (EVM_{RMS}) values are calculated from the deviated signals in the analyzer. Here, EVM_{RMS} is defined as

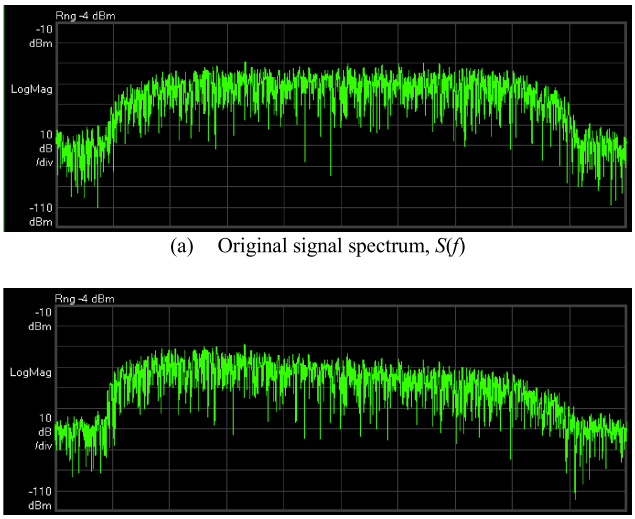

(a) Original signal spectrum, $S(f)$

(b) Signal spectrum after deviation, $G(f)$

Fig. 5 Spectrum examples for experimental investigation.

Table 1 Experimental parameters for analyzing signal quality degradation due to amplitude deviation.

Baud rate (Gbaud)		2, 4, 6, 8, 10
Roll-off factor		0.4
Bandwidth (GHz)		2.8, 5.6, 8.4, 11.2, 14.0
Header segments	Symbol length	90
	Modulation scheme	QPSK
Data segments	Symbol length	1958
	Modulation scheme	64QAM
Carrier frequency (GHz)		10
Amplitude deviation (dB/GHz)		0, 0.2, 0.4, 0.6, 0.8, 1.0

$$EVM_{RMS} = \frac{\sqrt{\frac{1}{N}\sum_{i=1}^{N}\left|S_{ideal,i} - S_{meas,i}\right|^2}}{\sqrt{\frac{1}{M}\sum_{i=1}^{M}\left|S_{ideal,i}\right|^2}} \tag{2}$$

where i and N denote the symbol index and number of symbols, respectively. Term M denotes the number of constellation points. Terms S_{ideal} and S_{meas} denote the locations of the ideal signal points and measured signal point, respectively.

Figures 5 show the example of the single-carrier original signal spectrum and the signal spectrum after the amplitude deviates.

As shown in Fig. 5, the original signal spectrum, which a carrier signal is modulated using the 64QAM modulation scheme by the transmission data, has amplitude flatness in the signal BW. However, the signal spectrum after the amplitude deviates has amplitude non-flatness. The signal quality degradation due to the amplitude deviation is investigated experimentally. Table 1 gives the investigation parameters. Test single-carrier transmission signals are modulated with 64QAM for data segments and QPSK for header segments. The header segments are employed for synchronization at an analyzer. The baud rates are 2 GHz, 4 GHz, 6 GHz, 8 GHz, and 10 GHz. Because roll-off factor α is fixed at 0.4, the actual signal bandwidths, BWs, are 2.8 GHz, 5.6 GHz, 8.4 GHz, 11.2 GHz, and 14.0 GHz, respectively, which are

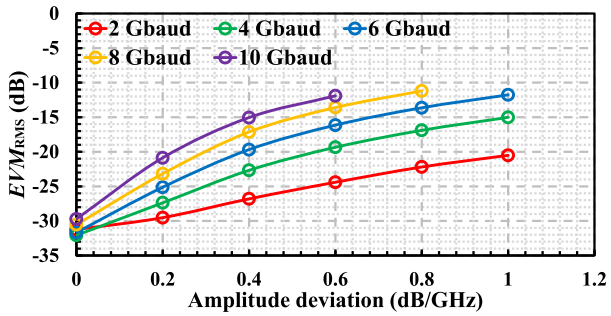

Fig. 6 Measured EVM_{RMS} corresponding to amplitude deviation against signal baud rates.

calculated using the equation below.

$$BW = Baud\ rate \times (1 + \alpha) \tag{3}$$

The first order amplitude deviation models which monotonically decrease with amplitude frequency characteristics of 0 dB/GHz, 0.2 dB/GHz, 0.4 dB/GHz, 0.6 dB/GHz, 0.8 dB/GHz, and 1.0 dB/GHz are employed for the simplest investigation. The center frequency of the test signal is 10 GHz.

Figure 6 plots the measured EVM_{RMS} values at each amplitude deviation. These results confirm that EVM_{RMS} deteriorates as the amplitude deviation increases, and the wider the signal BW becomes, the more severe the degradation. For the amplitude deviation of 0.8 and 1 dB/GHz for 10 Gbaud and that of 1 dB/GHz for 8 Gbaud, it is impossible to transmit any signal in the data segments due to synchronization failure caused by severe bit error of the signals in the header segments. Therefore, the spectrum non-flatness caused by the frequency response of the devices in the Tx must be compensated for single-carrier transmissions with a huge BW. The frequency response comprises the amplitude and phase characteristics. Needless to say, not only the amplitude frequency characteristics but also the phase frequency characteristics must be considered for equalization. The effect of considering both amplitude and phase characteristics in calculating the inverse frequency response are verified in [32]. Both the amplitude and phase characteristics should be corrected to obtain sufficient improvement.

3. Single-Carrier Transmission Experiments

3.1 Single-Carrier Transmission with Pre-Equalization

To confirm the feasibility of the proposed configuration, an experimental single-carrier transmission system including a Tx with the pre-equalizer and Rx without any equalizers is constructed as shown in Figs. 7. Table 2 gives the experimental parameters. The AWG generates a modified transmission signal for pre-equalization using the output signal of the Tx with frequency response non-flatness, $H_{tx}(f)$. Figure 8 shows a block diagram of the AWG in the proposed Tx. In the AWG, ${H_{tx}}^{-1}(f)$ is calculated from the feedback signal including a feature of $H_{tx}(f)$ using a zero-forcing algorithm.

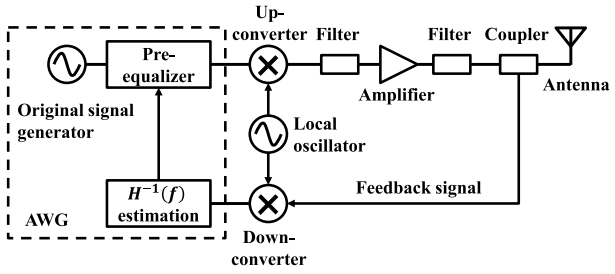

(a) Transmitter configuration

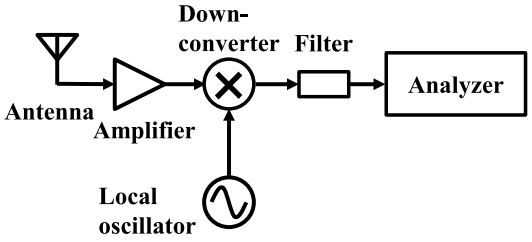

(b) Receiver configuration

Fig. 7 Block diagram of experimental single-carrier transmission system.

Table 2 Experimental parameters.

Baud rate (Gbaud)		2, 4, 6, 8, 10
Roll-off factor		0.4
Bandwidth (GHz)		2.8, 5.6, 8.4, 11.2, 14.0
Header segments	Symbol length	90
	Modulation scheme	QPSK
Data segments	Symbol length	1958
	Modulation scheme	64QAM
Carrier frequency of RF (GHz)		141.5

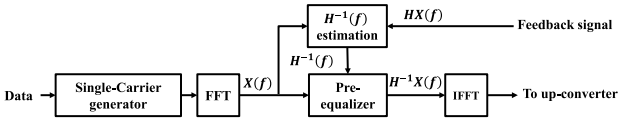

Fig. 8 Functional blocks in AWG for proposed transmitter.

Because the pre-equalization is processed in the frequency domain, the functions of the fast Fourier transform (FFT) and inverse FFT (IFFT) are included in the AWG. In this trial, time variance of the frequency response is not considered. Here, to evaluate the effects of pre-equalization for the Tx frequency response non-flatness, the frequency response of the Rx is calibrated before experiments.

The center frequency of the modified signal is 10 GHz with BWs corresponding to baud rates of 2 GHz, 4 GHz, 6 GHz, 8 GHz, and 10 GHz. Then the frequency of the modified signal is converted to 141.5 GHz by an up-converter with a local oscillator in Fig. 7 (a). The subsequent filter constrains unwanted emissions such as harmonics. After amplification by a PA, the original transmission signal is transmitted from an antenna because of pre-equalization using the feedback signal from the filtered output of the PA. The transmission signals have the roll-off factor, α, of 0.4, and the modulation schemes are 64QAM.

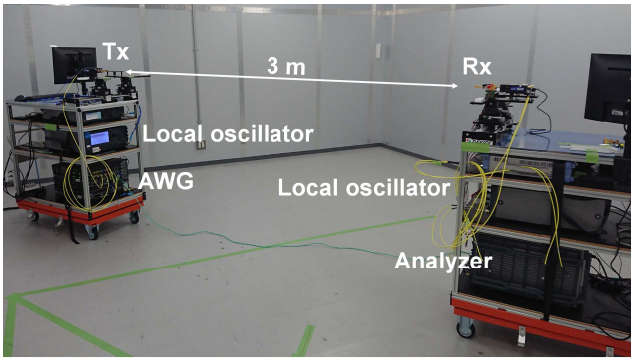

Fig. 9 Picture of experiment system.

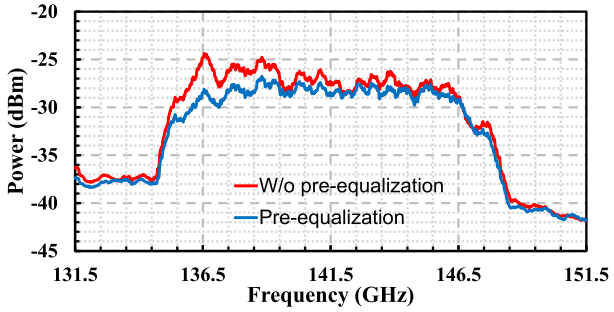

Fig. 10 Signal spectra for transmission systems with or without pre-equalization.

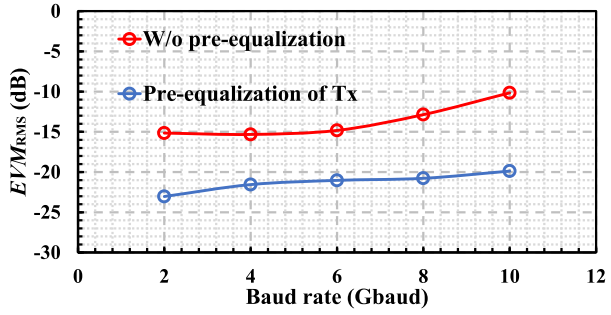

Fig. 11 Measured EVM_{RMS} for single-carrier (64QAM) transmission with/without pre-equalization.

Figure 9 shows a picture of the experiment system. There is a distance of 3 m between the Tx and Rx. Standard gain horn antennas are employed on both sides of the Tx and Rx. As shown in Fig. 9, the trial is conducted in a line-of-sight environment in an electromagnetically shielded room.

Figure 10 shows an example of the transmission signal spectra from the Tx antenna with or without Tx pre-equalization. The spectrum after pre-equalization becomes approximately 3 dB flatter than that without pre-equalization. We confirm that the flatness of the spectrum is improved after pre-equalization in the Tx.

Figure 11 shows measured EVM_{RMS} values for single-carrier (64QAM) transmission with or without pre-equalization in the Tx. According to Fig. 11, the EVM_{RMS} values for the transmission with pre-equalization exceed those without pre-equalization by more than 5 dB. Specially, the pre-equalization yields greater improvement at the baud rate of 8 Gbaud and 10 Gbaud due to a flatter spectrum as shown in Fig. 10.

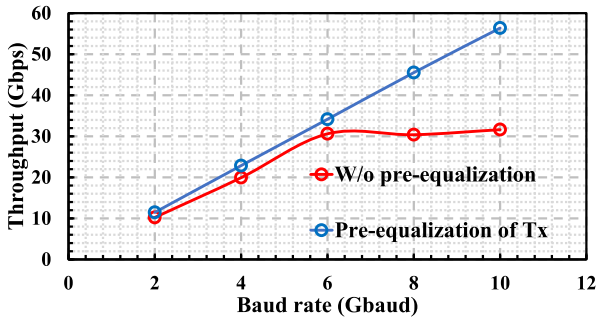

Fig. 12 Measured throughput for single-carrier (64QAM) transmission with/without pre-equalization.

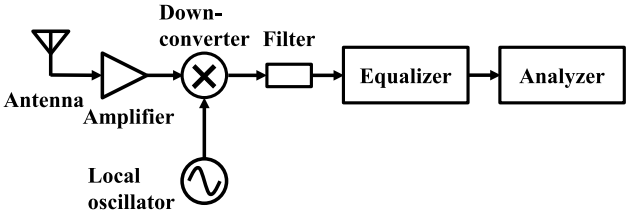

Fig. 13 Block diagram of Rx configuration with equalizer.

Figure 12 shows the measured throughput values for single-carrier (64QAM) transmission with or without Tx pre-equalization. The throughput, T, is calculated as

$$T = \mathit{Baud\ rate} \times \log_2 M \times (1 - \mathit{BER}) \tag{4}$$

In this experiment, no error correction code is used. According to Fig. 12, the throughput is improved by pre-equalization and 10-Gbaud transmission improves the throughput by approximately 25 Gbps.

3.2 Combining Single-Carrier Transmission with Pre-Equalization and Rx with Equalizer

In the previous section, the effects of pre-equalizing the frequency response non-flatness of the Tx are verified and confirmed. However, the pre-equalization does not equalize the frequency responses of the propagation channel and the Rx. In this section, the effect of pre-equalization in the Tx is verified when a conventional equalizer is also employed in the Rx. The Rx with the equalizer is constructed as shown in Fig. 13. Here, the total frequency response non-flatness of the propagation channel and the Rx is compensated for by the equalizer using the least mean square algorithm.

Figure 14 shows measured EVM_{RMS} values for single-carrier (64QAM) transmission with the equalizer in the Rx. The equalizer comprises a tapped delay line (TDL) and outputs a weighted sum of the values in the delay line. In this measurement, the TDL length for the equalizer in the Rx is 11 taps. According to Fig. 14, for 2 Gbaud and 4

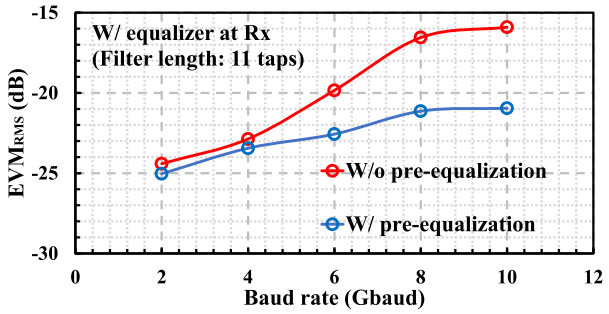

Fig. 14 EVM_{RMS} of each pre-equalization scheme with equalizer at Rx (Equalization filer length is 11 taps).

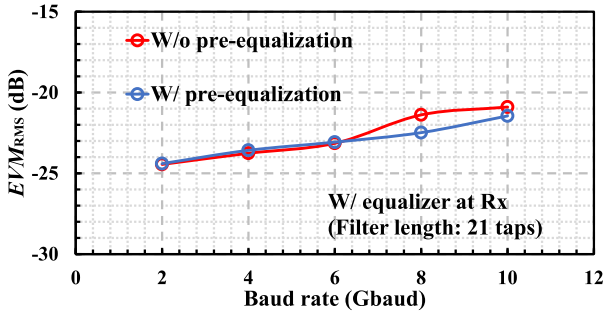

Fig. 15 EVM_{RMS} of each pre-equalization scheme with equalizer at Rx (Equalization filer length is 21 taps).

Gbaud transmission signals, pre-equalization provides little EVM_{RMS} improvement resulting from ISI equalization in the Rx. However, the proposed configuration yields improved EVM_{RMS} values for transmission signals above 6 Gbaud. This is why the equalizer in the Rx with the 11 taps is unable to equalize sufficiently the total frequency response non-flatness of the Tx, propagation channel, and Rx.

Figure 15 shows the measured EVM_{RMS} values for single-carrier (64QAM) transmission using the equalizer with a 21 taps in the Rx. If a sufficient number of taps can be provided in the equalizer in the Rx, the EVM_{RMS} values improve at high baud rates such as 8 GHz and 10 GHz.

Figure 16 shows the measured EVM_{RMS} values for single-carrier (64QAM) transmission with the baud rate of 10 GHz using the equalizer with the TDL in the Rx. The EVM_{RMS} values are plotted at each tap. In Fig. 16, 0 tap indicates the case where no equalization is performed. When the delay line length of the equalizer in the Rx is shorter than 21 taps, the pre-equalization scheme that compensates for the frequency response of the Tx is effective in improving the EVM_{RMS} values.

In other words, even if the length of the TDL is short, EVM_{RMS} degradation can be suppressed by pre-equalization in the Tx as shown in Fig. 16. The more taps that are equipped in the equalizer, the higher the computational complexity level becomes. If the degradation due to frequency response non-flatness of the Tx is compensated for in the Tx, the equalizer in the Rx is designed to compensate for only the

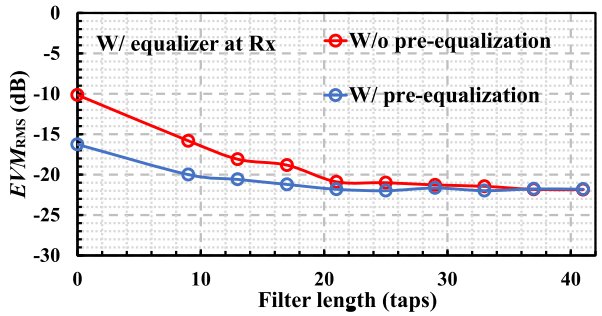

Fig. 16 EVM_{RMS} of signals with baud rate of 10 Gbaud for each pre-equalization scheme with equalizer at Rx.

frequency response of the propagation channel and Rx. The required calculation load for the equalizer is proportional to the cube of the filter length. For example, according to Fig. 16, the EVM_{RMS} value of -20 dB can be achieved at least 9 taps and 21 taps with and without pre-equalization, respectively. Therefore, since the proposed pre-equalization can make the calculation load approximately one-tenth, it is expected to reduce the power consumption corresponding to the reduction in the calculation load. Moreover, although the frequency response non-flatness depends on the Tx configuration, the pre-equalization in the Tx enables to design the Rx regardless of the Tx configuration for the transmission using the huge BW.

4. Conclusion

In this paper, a novel Tx configuration for an ultra-wideband transmission using a sub-THz frequency was proposed. The Tx employs a pre-equalization technique that compensates for the frequency response caused by implemented components in the operation band. To verify the feasibility of the proposed configuration, a single-carrier transmission system is configured and tested. Compared to a conventional Tx without pre-equalization, it is verified that the proposed Tx improves the error vector magnitude for single-carrier transmission with an ultra-wideband over 10 GHz regardless of whether or not there is an equalizer in the Rx. The proposed configuration can meet the demand of future ultra-wideband transmission systems for 6G.

Acknowledgments

This paper includes a part of the results from “R&D for Expansion of Radio Wave Resources (JPJ000254),” commissioned by The Ministry of Internal Affairs and Communications, Japan.

References

[1] W.K. Alsaedi, H. Ahmadi, Z. Khan, and D. Grace, “Spectrum options and allocations for 6G: A regulatory and standardization review,” IEEE Open Journal of the Communications Society, vol.4, pp.1787–1812, Aug. 2023.
[2] D.G.S. Pivoto, T.T. Rezende, M.S.P. Facina, R. Moreira, F. de

Oliveira Silva, K.V. Cardoso, S.L. Correa, A.V.D. Araujo, R.S. Silva, H. Scalco Neto, G.R.L. Tejerina, and A.M. Alberti, "A detailed relevance analysis of enabling technologies for 6G architectures," IEEE Access, vol.11, pp.89644–89684, 2023.

[3] W. Saad, M. Bennis, and M. Chen, "A vision of 6G wireless systems: Applications, trends, technologies, and open research problems," IEEE Netw., vol.34, no.3, pp.134–142, Oct. 2019.

[4] M. Giordani, M. Polese, M. Mezzavilla, S. Rangan, and M. Zorzi, "Toward 6G networks: Use cases and technologies," IEEE Commun. Mag., vol.58, no.3, pp.55–61, March 2020.

[5] C. Ranaweera, C. Lim, Y. Tao, S. Edirisinghe, T. Song, L. Wosinska, and A. Nirmalathas, "Design and deployment of optical x-haul for 5G, 6G, and beyond: Progress and challenges," Journal of Optical Communications and Networking, vol.15, no.9, pp.D54–D66, Sept. 2023.

[6] P. Mishra and G. Singh, "6G-IoT framework for sustainable smart city: Vision and challenges," IEEE Consum. Electron. Mag. (Early Access), pp.1–8, Aug. 2023.

[7] H.M.F. Noman, E. Hanafi, K.A. Noordin, K. Dimyati, M.N. Hindia, A. Abdrabou, and F. Qamar, "Machine learning empowered emerging wireless networks in 6G: Recent advancements, challenges and future trends," IEEE Access, vol.11, pp.83017–83051, Aug. 2023.

[8] A. Alkhateeb, S. Jiang, and G. Charan, "Real-time digital twins: Vision and research directions for 6G and beyond," IEEE Commun. Mag., vol.61, no.11, pp.128–134, 2023.

[9] M.A. Saeidi, H. Tabassum, and M.-S. Alouini, "Multi-band wireless networks: Architectures, challenges, and comparative analysis," IEEE Commun. Mag., vol.62, no.1, pp.80–86, 2024.

[10] J. Li, S. Dang, M. Wen, Q. Li, Y. Chen, Y. Huang, and W. Shang, "Index modulation multiple access for 6G communications: Principles, applications, and challenges," IEEE Netw., vol.37, no.1, pp.52–60, Jan./Feb. 2023.

[11] A. Fayad, T. Cinkler, and J. Rak, "5G/6G optical fronthaul modeling: Cost and energy consumption assessment," Journal of Optical Communications and Networking, vol.15, no.9, Sept. 2023.

[12] NTT DOCOMO, INC., "White paper 5G evolution and 6G," Version 4.0, Jan. 2022.

[13] P.K. Agyapong, M. Iwamura, D. Staehle, W. Kiess, and A. Benjebbour, "Design considerations for a 5G network architecture," IEEE Commun. Mag., vol.52, no.11, pp.65–75, Nov. 2014.

[14] C.E. Shannon, "The zero-error capacity of a noisy channel," IRE Trans. Inf. Theory, vol.IT-2, no.3, pp.8–19, Sept. 1956.

[15] J. Ma, "Modified Shannon's capacity for wireless communication," IEEE Microw. Mag., vol.22, no.9, pp.97–100, Aug. 2021.

[16] P. Yang, Y. Xiao, M. Xiao, and S. Li, "6G wireless communications: Vision and potential techniques," IEEE Netw., vol.33, no.4, pp.70–75, July 2019.

[17] T.S. Rappaport, Y. Xing, O. Kanhere, S. Ju, A. Madanayake, S. Mandal, A. Alkhateeb, and G.C. Trichopoulos, "Wireless communications and applications above 100 GHz: Opportunities and challenges for 6G and beyond," IEEE Access, vol.7, pp.78729–78757, June 2019.

[18] Mingquan Bao, et al., "G-band power amplifiers in 130 nm InP technology," 2020 15th European Microwave Integrated Circuits Conference (EuMIC), pp.5–8, Jan. 2021.

[19] H. Hamada, T. Tsutsumi, H. Matsuzaki, T. Fujimura, I. Abdo, A. Shirane, K. Okada, G. Itami, H.-J. Song, H. Sugiyama, and H. Nosaka, "300-GHz-band 120-Gb/s wireless front-end based on InP-HEMT PAs and mixers," IEEE J. Solid-State Circuits, vol.55, no.9, pp.2316–2335, Sept. 2020.

[20] J.S.-C. Chien, W. Lee, and J.F. Buckwalter, "High-efficiency 200-GHz neutralized common-base power amplifiers in 250-nm InP HBT," IEEE Journal of Microwaves, vol.3, no.2, pp.715–725, March 2023.

[21] S. Gielen, Y. Zhang, M. Ingels, and P. Reynaert, "A D-band 20.4 dBm OP1dB transformer-based power amplifier with 23.6% PAE in a 250-nm InP HBT technology," 2023 IEEE Radio Frequency Integrated Circuits Symposium (RFIC), pp.309–312, 2023

[22] X. Li, W. Chen, H. Wu, S. Li, X. Yi, R. Han, and Z. Feng, "A 110-to-130 GHz SiGe BiCMOS Doherty power amplifier with a Slotline-based power combiner," IEEE J. Solid-State Circuits, vol.57, no.12, pp.3567–3581, Dec. 2022.

[23] S.H. Han and J.H. Lee, "An overview of peak-to-average power ratio reduction techniques for multicarrier transmission," IEEE Wireless Commun., vol.12, no.2, pp.56–65, April 2005.

[24] E. Song, S. Member, J. Kim, and J. Kim, "A Passive Equalizer Optimization Method Based on Time-Domain Inter-Symbol Interference (ISI) Cancellation Technique," IEEE Trans. Electromagn. Compat., vol.60, no.3, pp.807–810, March 2018.

[25] S. Kanthalue, P. Nanan, "Pre- and post-equalization technique combining for wireless communications," The International Conference on Information Networking 2013 (ICOIN), pp.336–340, Jan. 2013.

[26] F. Adachi, K. Takeda, and H. Tomeba, "Multi-antenna pre-equalization for single carrier TDD system," 2005 IEEE 61st Vehicular Technology Conference, pp.452–456, 2005.

[27] J. Li, X. Sha, and X. Fang, "WFRFT based multi-antenna transmission method with pre-equalization," 2018 14th IEEE International Conference on Signal Processing (ICSP), pp.1056–1059, 2018.

[28] S.-Y. Sun, W.-X. Meng, and H.-H. Chen, "Uplink pre-equalization for CC-CDMA systems under frequency selective fading," Proc. IEEE ICC 2013, pp.5317–5321, 2013.

[29] B.A. Cevikgibi, A.M. Demirtas, T. Girici, and H. Arslan, "Inter-numerology interference pre-equalization for 5G mixed-numerology communications," 2022 IEEE 95th Vehicular Technology Conference: (VTC2022-Spring), 2022.

[30] S. Wen, G. Liu, C. Liu, H. Qu, L. Zhang, and M.A. Imran, "Joint precoding and pre-equalization for faster-than-Nyquist transmission over multipath fading channels," IEEE Trans. Veh. Technol., vol.71, no.4, pp.3948–3963, April 2022.

[31] W.-C. Chen, C.-D. Chung, and P.-H. Wang, "Pre-equalized and spectrally precoded OFDM," IEEE Trans. Veh. Technol, vol.71, no.7, pp.7472–7486, July 2022.

[32] H. Yamamoto, A. Fukuda, S. Aoki, H. Hamada, H. Okazaki, and Y. Suzuki, "Wideband Single Carrier Transmitter Configuration Equalizing Non-flat Frequency Response," 2022 27th Asia Pacific Conference on Communications (APCC), pp.209–213, Oct. 2022.

Atsushi Fukuda received the B.E. and M.E. degrees from the Tokyo University of Science, Tokyo, Japan, in 1997 and 1999, respectively, and the Ph.D. degree from Hokkaido University, Sapporo, Japan, in 2012. In 1999, he joined NTT DOCOMO, INC., Yokosuka, Japan, where he was involved in research on RF circuits and development on base station equipment for mobile communication systems. His current research interests include sub-THz communication systems for 6G. He is a senior member of the IEICE. He was a recipient of the 2011 IEICE Achievement Award and the 2012 IEICE Best Paper Award.

Hiroto Yamamoto received the B.S. and M.S. degrees in electrical engineering from Tokyo University of Science in 2018 and 2020, respectively. He joined NTT DOCOMO, INC., Yokosuka-shi, Japan, in 2020. His current research interests include wireless communication systems.

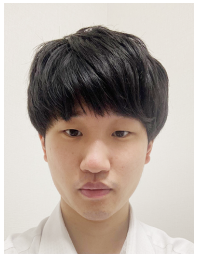

Junya Matsudaira received the B.S. and M.S. degrees in electrical engineering from Osaka University in 2017 and 2023, respectively. He joined NTT DOCOMO, INC., Yokosuka-shi, Japan, in 2023. His current research interests include wireless communication systems.

Sumire Aoki received the B.S. and M.S. degrees in physics from Tokyo Metropolitan University in 2010 and 2012, respectively. She joined NTT DOCOMO, INC., Yokosuka-shi, Japan, in 2023. Her current research interests include wireless communication systems.

Yasunori Suzuki received the B.E. and M.E. degrees from Nagaoka University of Technology, Niigata, Japan, in 1993 and 1995, respectively, and the Ph.D. degree from Hokkaido University, Sapporo, Japan, in 2011. In 1995, he joined NTT Mobile Communications Network, Inc. (now NTT DOCOMO, INC.) where he was engaged in research on base station equipment for mobile communications. He is currently a Senior Manager of 6G Network Innovation Department.